Cation distribution and mixing thermodynamics in Fe/Ni thiospinels

Saima Haider *, Ricardo Grau-Crespo, Antony J. Devey, Nora H. de Leeuw

Department of Chemistry, University College London, 20 Gordon Street, London WC1H 0AJ, United Kingdom

Abstract

The structural analogy between Ni-doped greigite minerals (Fe_3S_4) and the $(Fe, Ni)S$ clusters present in biological enzymes has led to suggestions that these minerals could have acted as catalysts for the origin of life. However, little is known about the distribution and stability of Ni dopants in the greigite structure. We present here a theoretical investigation of mixed thiospinels $(Fe_{1-x}Ni_x)_3S_4$, using a combination of density functional theory (DFT) calculations and Monte Carlo simulations. We find that the equilibrium distribution of the cations deviates significantly from a random distribution: at low Ni concentrations, Ni dopants are preferably located in octahedral sites, while at higher Ni concentrations the tetrahedral sites become much more favourable. The thermodynamic mixing behaviour between greigite and polydymite (Ni_3S_4) is dominated by the stability field of violarite ($FeNi_2S_4$), for which the mixing enthalpy exhibits a deep negative minimum. The analysis of the free energy of mixing shows that Ni doping of greigite is very unstable with respect to the formation of a separate violarite phase. The calculated variation of the cubic cell parameter with composition is found to be non-linear, exhibiting significant deviation from Vegard's law, but in agreement with experiment.
© 2012 Elsevier Ltd. All rights reserved.

1. INTRODUCTION

Greigite is the iron sulphide mineral Fe_3S_4 (Rickard and Luther, 2007), which consists of a mixture of Fe^{3+} and Fe^{2+} ions bonded to S^{2-} ions. It has a cubic unit cell with cell parameter $a = 9.876$ Å and $Fd3m$ space group symmetry (Skinner et al., 1964). Classified as the sulphur analogue of magnetite, the cubic unit cell of this thiospinel (Fig. 1) consists of eight AB_2S_4 units (Vaughan and Craig, 1978), with trivalent Fe cations occupying the tetrahedral (A) sites, and both trivalent and divalent Fe cations located in the octahedral (B) sites (Vaughan et al., 1971; Devey et al., 2009).

Greigite formation in nature may occur via the reduction of iron solutions by the bacteria *Desulphibrio desulphi-ricans* (Freke and Tate, 1961), but only under anaerobic conditions in H_2S-rich waters (Hoffmann, 1992). Iron–nickel sulphides have been implicated in the origin of life, based on the observation that these minerals contain iron-sulphide clusters akin to those found in a number of contemporary enzymes known to catalyse similar reactions to those involved in primordial metabolism (Huber and Wächtershäuser, 1997), specifically the acetyl-coenzyme-A (CoA) pathway, which involves the overall conversion of two molecules of carbon dioxide (CO_2) into an acetate group, with water as a by-product (Ferry, 1995; Huber and Wächtershäuser, 1997; Russell and Martin, 2004). Nickel is a vital component required for such catalytic activity, and it is also a known impurity in greigite (Rickard and Luther, 2007). The structural resemblance between the NiFeS clusters in the active sites of many biological enzymes and nickel-doped iron sulphide minerals such as greigite (Russell and Martin, 2004), led to the proposal of the iron–sulphur membrane theory (Russell and Hall, 1997),

* Corresponding author.
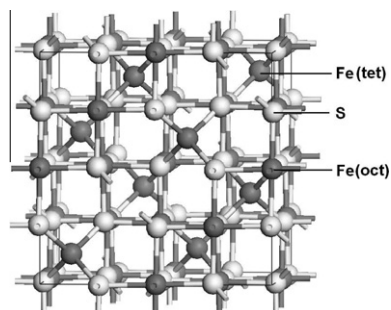 *E-mail address:* uccasah@live.ucl.ac.uk (S. Haider).

Fig. 1. Greigite as seen along the *c*-axis; S in light grey, Fe in dark grey.

which suggests that life arose at a redox and pH front on the Hadean ocean floor (∼4 billion years ago). According to these suggestions, the meeting between the alkaline hydrothermal front generated in the oceanic crust with the acidic oceanic fluid led to a spontaneous precipitation of FeS and NiS membranes or 'bubbles', which formed via a reaction between dissolved transition metals from the ocean, such as iron, with bisulphide contained in the hydrothermal fluid (Russell and Martin, 2004). These membranes are then supposed to have undergone a geochemical transformation to form greigite (Fe_3S_4) and violarite (Fe-Ni_2S_4) (Cody, 2004). The reducing environment necessary for the conversion of CO_2 to CO is readily achieved via a switch in valency of Fe ions from II (ferrous) to III (ferric) (Russell and Martin, 2004). FeS membranes formed at the hydrothermal front would certainly have contained trace amounts of Ni, probably sufficient to cleave the hydrothermal hydrogen at the nickel site producing hydride (Russell and Hall, 1997), an important step in the present-day acetyl-CoA pathway. We know nickel to have an important role in biological catalysis, and its inclusion in enzymes is attributed to its flexibility in coordination and ability to transfer quickly between either of the oxidation states (I) (II) and (III) (Ragsdale, 2009).

In order to develop further the chemical analogy between FeNi enzymes and FeNi-sulphide minerals, a comparison between the coordination environment of the cations in the enzymes and the minerals would be useful. In NiFe hydrogenases, a class of enzymes responsible for the conversion of molecular hydrogen into a proton and hydride (Russell and Hall, 1997; Volbeda and Fontecilla-Camps, 2003; Canaguier et al., 2008; Ragsdale, 2009), the coordination of nickel in the active site is always lower than that of iron. For instance, when the enzyme is in the oxidised state, Ni is in square-planar coordination, while Fe is square-pyramidal; in the reduced state, Ni exhibits a square-pyramidal coordination, and the Fe has an octahedral geometry (Volbeda et al., 1995; Volbeda and Fontecilla-Camps, 2005; Canaguier et al., 2008). In the case of CODH (carbon monoxide dehydrogenase – responsible for the catalysis of CO_2 to CO (Russell and Martin, 2004; Ragsdale, 2009)), Ni is in a tetrahedrally distorted square-planar coordination, with the proximal Fe also displaying tetrahedral geometry (Dobbek et al., 2001; Svetlitchnyi et al., 2004; Gencic et al., 2010). This is also the case for the distal Ni in acetyl coenzyme-A synthetase (ACS) (the

enzyme which acts to combine the resultant CO with a methyl group (Volbeda and Fontecilla-Camps, 2005)), where Ni exhibits a square-planar geometry (Lindahl, 2004). From these observations, it seems that the analogy between the sulphide minerals and the enzymes is closer when Ni is preferentially located in tetrahedral sites of the greigite structure, and indeed, this agrees with the representation made of the Ni-doped greigite structure in the original paper on the iron–sulphur membrane theory by Russell and Martin (2004). However, so far the coordination environment of Ni in greigite has not been investigated.

In this work, we present a theoretical investigation of the partitioning of Ni over the tetrahedral and octahedral sites of greigite, for which we find a strong composition dependence. We also discuss the thermodynamics of mixing in the (Fe, Ni)$_3S_4$ system, to explain why violarite (FeNi$_2S_4$) is the most common composition in the solid solution series between greigite and polydymite (Ni$_3S_4$), while low Ni/Fe ratios are much less abundant (Misra and Fleet, 1974).

2. METHODOLOGY

2.1. Density functional theory

We have employed density functional theory (DFT) calculations to obtain the energies and equilibrium geometries of the Fe/Ni thiospinels, using the Vienna *ab initio* simulation package (VASP) (Kresse and Hafner, 1993, 1994; Kresse and Furthmüller, 1996). This approach has already been used successfully in the modelling of a number of iron sulphide minerals (e.g. Rohrbach et al. (2003), Devey et al. (2008, 2009), Devey and de Leeuw (2010)). All calculations are performed within the generalised gradient approximation (GGA), with the exchange–correlation functional developed by Perdew et al. (1992), and the spin interpolation formula of Vosko et al. (1980). Following previous work (Devey et al., 2009), a Hubbard correction with $U_{eff} = 1$ eV was applied to the Fe d orbitals to improve the description of the electron localisation.

The valence orbitals are calculated as linear combinations of plane waves, and the size of the basis set is determined by a cutoff energy (400 eV in our case). The core levels are kept 'frozen' during the calculations, which in this instance consist of orbitals up to, and including 3p for Fe and Ni, and 2p for S. The interactions between the valence electrons and core orbitals are described using the projector augmented wave (PAW) method (Blöchl, 1994) in the implementation of Kresse and Joubert (1999). All calculations were performed in a cell with composition Fe$_{24-n}$Ni$_n$S$_{32}$. A Monkhorst–Pack grid (Monkhorst and Pack, 1976) of $4 \times 4 \times 4$ was employed to sample the Brillouin zone. All calculations were spin-polarised, and the magnetic moments of the octahedral and tetrahedral sublattice were always given opposite orientations, in agreement with experimental evidence (Devey et al., 2009).

2.2. Statistical mechanics of configurations

For low Ni concentrations, we have evaluated *all* the different configurations of Fe/Ni substitutions in the

simulation cell, using the site occupancy disorder (SOD) program (Grau-Crespo et al., 2007), which has been employed previously in simulations of the ionic distribution in minerals (e.g. Grau-Crespo et al. (2003, 2004, 2010) and Ruiz-Hernandez et al. (2010)). This program uses the crystal symmetry to reduce the configurational space that must be evaluated with the DFT calculations, selecting only the symmetrically inequivalent configurations. We can assign a probability of occurrence to each inequivalent configuration m ($m = 1, \ldots, M$) with degeneracy Ω_m as:

$$P_m = \frac{1}{Z} \Omega_m \exp \frac{-E_m}{k_B T} \tag{1}$$

where T is the temperature, k_B is Boltzmann's constant and equal to 8.6173×10^{-5} eV K^{-1}, E_m is the energy of the configuration, and Z is the partition function which ensures that the sum of probabilities is equal to 1. We can then calculate the configurational average of any quantity Q (e.g. energy, cell parameter, etc.) using:

$$\langle Q \rangle = \sum_{m=1}^{M} P_m Q_m \tag{2}$$

where Q_m is the quantity value for configuration m. However, at high dopant concentrations the cost of calculating the full configurational spectrum becomes prohibitive. We therefore introduce a model based on nearest-neighbour (NN) concentration-dependent interactions (hereafter referred to as the NN model), which is fitted to the results of the DFT calculations and then employed to evaluate the energies of configurations sampled with a Monte Carlo procedure (Lavrentiev et al., 2003; Purton et al., 2005). The acceptance or rejection of each configuration is based on the Metropolis algorithm (Metropolis et al., 1953), which involves the calculation of the energy difference, ΔE, between the particular configuration i and the previously accepted one:

$$\Delta E = E_i - E_{(i-1)} \tag{3}$$

If $\Delta E < 0$, then the configuration is accepted. Otherwise, a random number r is generated (such that $0 < r < 1$), and the condition of acceptance then becomes:

$$r < \exp(-\Delta E / k_B T) \tag{4}$$

Within this procedure, a technique known as importance sampling is utilised, whereby the generation of our random configurations is biased in such a way that the previously accepted configuration is used as a template for the new one. In our case, the modification introduced at each step is that one Ni and one Fe ion swap sites within the lattice. In order to eliminate the impact of uncommon or extreme readings on the final result, the simulation is allowed to run and equilibrate for some time before we collect data from it. Convergence is monitored by checking the deviation in energy of the new configuration from the previously calculated average. Once below a certain threshold, the calculation is accepted to have converged.

3. RESULTS AND DISCUSSION

3.1. Ni doping at low concentrations

We first discuss the case of low concentrations of nickel in greigite (0–3 ions per unit cell, or fractional concentrations $x \leqslant 0.125$ in $(Ni_xFe_{1-x})_3S_4$), for which we were able to obtain the full configurational spectrum via DFT calculations.

In the case of one Ni in the unit cell, there are only two possible substitutional configurations: in an octahedral or in a tetrahedral site. The energy of the substitution in the tetrahedral site is $\Delta\varepsilon = 0.439$ eV higher than in the octahedral site. In order to interpret this energy difference, we can calculate the occupancies x_A and x_B of the two types of sites in the limit of very low overall concentrations x from the equation:

$$\frac{x_A}{x_B} = e^{-\frac{\Delta\varepsilon}{RT}} \tag{5}$$

which together with the condition

$$\frac{1}{3}x_A + \frac{2}{3}x_B = x \tag{6}$$

leads to

$$x_A = \frac{3xe^{-\frac{\Delta\varepsilon}{RT}}}{2 + e^{-\frac{\Delta\varepsilon}{RT}}}; \quad x_B = \frac{3x}{2 + e^{-\frac{\Delta\varepsilon}{RT}}} \tag{7}$$

In real samples the distribution of cations is unlikely to be equilibrated at room temperature because the thermal energy is not enough to overcome the activation barriers for cation diffusion. We therefore discuss here the equilibrium distribution of cations at a representative temperature, $T = 600\ K$, which is chosen close to the maximum temperature at which the whole $(Ni_xFe_{1-x})_3S_4$ series is known to be stable (the pure Ni end-member is stable only up to ≈ 630 K (Vaughan and Craig, 1985)). At this temperature, $x_A = 0.0003x$, which means that in the limit of low concentrations only 0.01% of the total Ni content would be in tetrahedral sites.

For two or more Ni atoms per unit cell, the analysis cannot be done in terms of one energy difference, because there are several possible configurations for the ions in the cell (Table 1). For example, for 2 Ni atoms in the cell there are $24!/(22!2!) = 276$ combinations, of which 7 are symmetrically different. These include configurations with both Ni in octahedral positions, configurations with both Ni in tetrahedral positions and configurations with one octahedral and one tetrahedral Ni. In this case, the effective Ni occupancy of the tetrahedral (A) sites can be obtained as an average (Eq. (2)) of the Ni tetrahedral occupancies of the configurations:

$$x_A = \frac{1}{8} \sum_{m=1}^{M} P_m t_m \tag{8}$$

where t_m is the number of tetrahedral Ni atoms per cell in configuration m, which has probability P_m (Eq. (1)). At 600 K and Ni concentrations $x = 0.0833$ and 0.1250 (2 and 3 Ni per cell), the tetrahedral site occupancies are

Table 1
Number of cation configurations as a function of the total number n of Ni ions per unit cell.

n	Total number of configurations	Symmetrically inequivalent configurations
1	24	2
2	276	7
3	2024	25
4	10,626	97
5	42,504	297
6	134,596	853

1.4×10^{-3} and 1.2×10^{-2}, which correspond to 0.6% and 3.3% of the total Ni content, respectively.

It is therefore clear that, although Ni strongly prefers to occupy octahedral positions when substituted at low concentrations, an increase in the overall concentration leads to an increase in the fraction of Ni occupying tetrahedral positions. It is interesting to investigate whether this trend continues for higher Ni concentrations.

3.2. Heavy Ni-doping: Monte Carlo simulations

At higher dopant concentrations (more than 3 Ni ions per cell, or $x > 0.125$), it becomes too expensive to perform DFT calculations of the entire configurational spectrum, due to the large number of possible configurations (see Table 1). We therefore have used the data obtained from our DFT calculations to fit a simplified interaction model for a rapid evaluation of energies. The model is based on an Ising-type Hamiltonian with three types of nearest-neighbour (NN) interactions and separate concentration-dependent substitution energies for tetrahedral (A) and octahedral (B) sites:

$$E = E_o + N_A \varepsilon_A + N_B \varepsilon_B + N_{AA} J_{AA} + N_{BB} J_{BB} + N_{AB} J_{AB} \quad (9)$$

where N_A and N_B refer to the number of Ni ions in A and B sites, and N_{AA}, N_{BB} and N_{AB} refer to the number of tetrahedral–tetrahedral, octahedral–octahedral and tetrahedral–octahedral nearest-neighbour Ni–Ni pairs. These parameters are specific for each configuration. E_o is the energy of un-doped (pure iron) greigite, and the constants J then refer to the interaction energies between Ni ions in the corresponding NN sites. ε_A and ε_B are the costs of individual Ni substitutions in sites A and B, respectively, and these values are allowed to vary linearly with concentration as:

$$\varepsilon_A = \varepsilon_A^o (1 + \alpha x); \quad \varepsilon_B = \varepsilon_B^o (1 + \beta x) \quad (10)$$

where ε_A^o and ε_B^o are the costs of placing a Ni in the A or B site in the limit of low concentrations. This leads to an energy model with a total of seven parameters. The DFT data used for the fitting consisted of all configurations with $n = 0 - 3$ Ni per unit cell as discussed above; all configurations with $4 \leqslant n \leqslant 8$ and either purely tetrahedral or purely octahedral occupancy; and a random selection of tetrahedral/octahedral mixed occupancy configurations for each composition. The final fitted values were $\varepsilon_A^o = 2.590$ eV, $\varepsilon_B^o = 2.091$ eV, $\alpha = -1.02741$, $\beta = 0.07771$, $J_{AA} = 0.05465$ eV, $J_{BB} = -0.02997$ eV, $J_{AB} = 0.05290$

eV, while E_o was taken directly from the DFT calculation of pure greigite. Fig. 2 shows that this NN interaction model accounts very well for the energy differences between configurations.

We then used this NN model to run Monte Carlo simulations at 600 K for concentrations $0 \leqslant x \leqslant 0.333$. Averages of energies and tetrahedral occupancies could then be extracted from the accepted configurations at each concentration. The calculated tetrahedral/octahedral partition for the whole range of concentrations is shown in Fig. 3, where we show the total Ni concentration (x) as a sum of both tetrahedral ($\frac{1}{3}x_A$) and octahedral ($\frac{2}{3}x_B$) contributions. We also illustrate the distribution of cations that is expected in the full disorder limit, where the concentration of nickel in the A sites is always one-third of the total nickel concentration, as well as the Monte Carlo result at 600 K, which deviates significantly from the random distribution. As we discussed above, at low Ni concentrations, B site substitutions are strongly favoured, while at higher concentrations there is a greater proportion of nickel ions in the A sites than in the B sites. The change in site preference occurs between $x = 0.20$ and $x = 0.25$. At $x = 1/3$, 87% of the Ni is located in tetrahedral sites. The plateau in the amount of tetrahedral Ni near $x = 1/3$ appears because of the filling of the tetrahedral sites. The high tetrahedral occupancy of Ni at high concentrations is consistent with observations that the mineral violarite $FeNi_2S_4$, with even higher Ni/Fe ratio, has only Ni in its tetrahedral sites (Tenailleau et al., 2006; Waldner, 2009).

3.3. Mixing thermodynamics

We now consider the enthalpy of mixing greigite and polydymite (Ni_3S_4):

$$\Delta H_{mix} = E[(Fe_{1-x}Ni_x)_3S_4] - (1-x)E[Fe_3S_4] - x[Ni_3S_4] \quad (11)$$

where we have ignored zero-point energy, heat capacity and pressure–volume contributions to the mixing enthalpy, which are typically small. The result is shown in Fig. 4a, including data obtained from both DFT and the NN interaction model. The energies of violarite, polydymite and Fe-doped polydymite were obtained directly from DFT calculations. In the case of violarite, the energy is a Boltzmann-weighted average of 97 configurations.

It is clear that violarite ($x = 0.666$) is the most energetically stable member of the (Fe, Ni)S solid solution series, with a very negative enthalpy of mixing of -15 kJ/mol, while Ni-doped greigite has a positive enthalpy of mixing. In order to obtain the maximum concentration of Ni dopants that is stable in greigite with respect to separation into violarite, it is convenient to write the formula for Ni-doped greigite as $Fe(Fe_{1-y}Ni_y)_2S_4$, where $y = \frac{3x}{2}$. Now $y = 0$ corresponds to greigite and $y = 1$ to violarite. The mixing enthalpy between greigite and violarite is shown in the inset in Fig. 4a. $\Delta H_{mix}(y)$ is positive, at least for all values of y studied here ($0 < y < 0.5$). At low concentrations, the dependence with y is linear with slope $W = 38.9$ kJ/mol. This large value (compared to RT) indicates that it is energetically unfavourable to move Ni from violarite to

greigite. We can estimate the maximum concentration of Ni that is stable in greigite from the minimum of the mixing free energy:

$$\Delta G_{mix}(y) = Wy - T\Delta S_{mix}(y) \quad (12)$$

where we have inserted the linear expression for the mixing enthalpy because the minimum can be expected to occur at low concentration due to the large W value. The mixing entropy can then be obtained from the configurational entropies of Ni-doped greigite and violarite (there is no configurational entropy in pure greigite), ignoring the small vibrational contributions, as:

$$\Delta S_{mix}(y) = S[Fe(Fe_{1-y}Ni_y)_2S_4] - yS[FeNi_2S_4] \quad (13)$$

where

$$S[Fe(Fe_{1-y}Ni_y)_2S_4] = -2k_B[y\ln y + (1-y)\ln(1-y)] \quad (14)$$

is the entropy associated with the disorder of Ni dopants in greigite, assuming they are all in octahedral sites (which is accurate at very low concentrations as seen above), and

$$S[FeNi_2S_4] = 2k_B \ln 2 \quad (15)$$

is the entropy of the disorder in the octahedral sites of violarite, which are occupied by Ni and Fe in a 50:50 proportion. The factor of 2 in Eqs. (14) and (15) accounts for the presence of two octahedral sites in each formula unit. The mixing free energy at $T = 600$ K has a minimum at approximately $y = 0.01$ $(Fe(Fe_{0.99}Ni_{0.01})_2S_4$ or Ni:Fe = 1:150), where Ni is mainly octahedral. This corresponds to the maximum equilibrium concentration (solubility) of Ni in greigite. Since most Ni is in octahedral sites at any reasonably low temperature and the Ni–Ni interaction is negligible at low concentrations, W does not vary appreciably with temperature and we can estimate the solubilities in a small range of temperatures, as shown in Fig. 4b. Although the solubility increases with temperature, even at 700 K the maximum Ni:Fe ratio in thermodynamic equilibrium is around 1:87. The consideration of higher temperatures is not relevant, as we have already discussed that the (Fe, Ni)S solid solution series will not be stable at such high temperatures (Vaughan and Craig, 1985).

The analysis above shows that Ni doping of greigite is thermodynamically very unfavourable with respect to the competitive formation of violarite $FeNi_2S_4$. Metastable incorporation beyond these limits is possible, as occurs in many minerals due to kinetic control of mineral growth. However, our results indicate that low Ni/Fe thiospinels would not be very abundant, and there is a notable lack of documentation on any such minerals being found in nature.

3.4. Variation of bond lengths and cell parameter with composition

Table 2 shows the bond lengths of Fe–S/Ni–S obtained from our DFT optimisations of pure greigite, polydymite, and greigite with one nickel substituted in place of a tetrahedral or octahedral iron. As we can see, inclusion of one Ni in either of the lattice sites in greigite leads to a de-
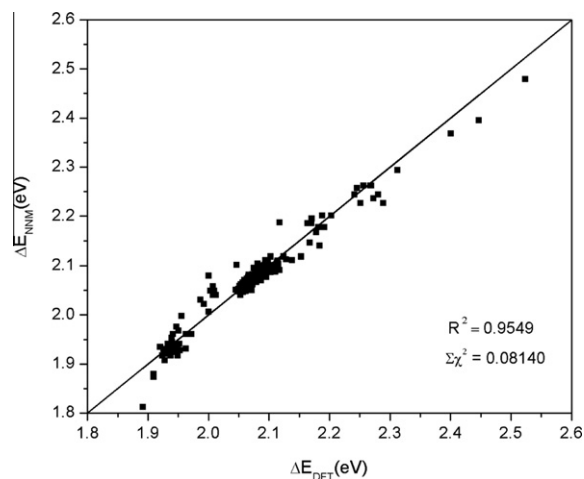

Fig. 2. Comparison between the energies per Ni substitution as calculated with DFT and those calculated with a nearest-neighbour interaction model (NNM). R^2 is the linear correlation coefficient, which measures the strength of correlation between the variables. $\Sigma\chi^2$ is the residual sum of squares, and is a measure of the discrepancies between the NNM and the DFT results.
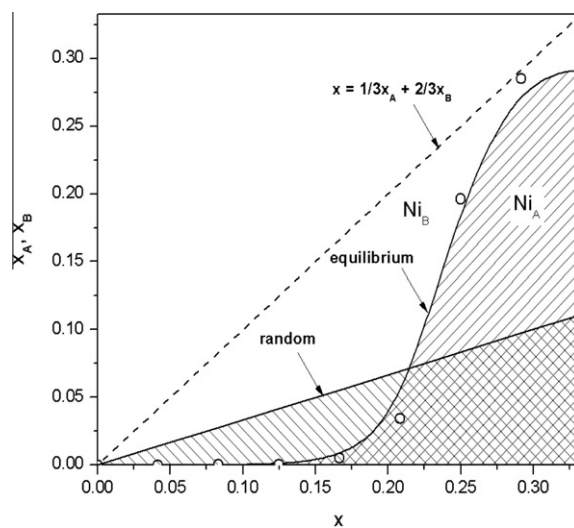

Fig. 3. Equilibrium distribution of Ni ions over tetrahedral and octahedral sites as a function of the total Ni concentration (x) at $T = 600$ K, in comparison with the random distribution ($T \to \infty$). The open circles are values obtained from the Monte Carlo simulations.

crease in the equivalent cation–sulphur bond length in pure greigite, although the bond distance is still greater than those Ni–S bonds found in polydymite. Yet the effect of Ni substitution on the adjacent Fe–S bonds varies depending on which lattice site is occupied by the dopant. When Ni is substituted in the tetrahedral site, the distance between the Fe coordinated to the same S as Ni also decreases. However, when Ni occupies an octahedral site, then the surrounding Fe–S bonds will be slightly longer than those found in pure greigite, effectively counteracting the decrease in bond length caused by Ni substitution. This effect ex-
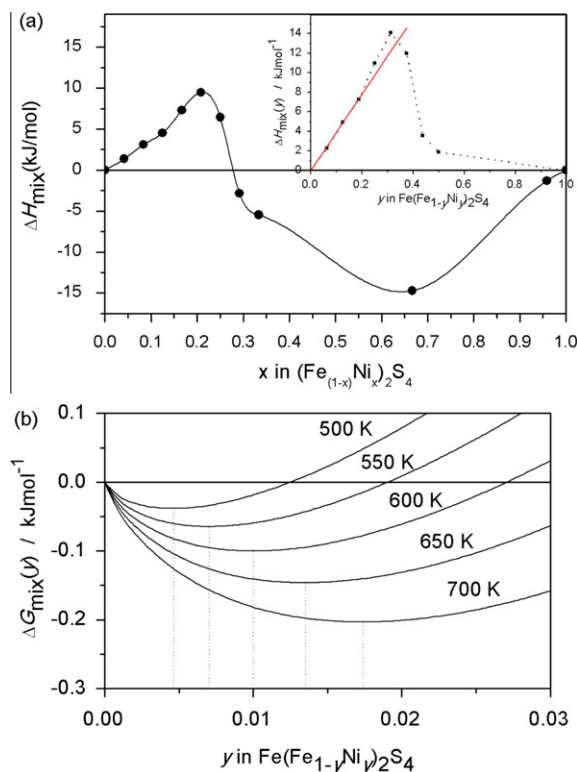
Fig. 4. (a) The energy of mixing $\Delta H_{mix}(x)$ calculated per formula unit with respect to greigite ($x = 0$) and polydymite ($x = 1$) ($x = 0.666$ corresponds to violarite). Inset: $\Delta H_{mix}(y)$ calculated per formula unit with respect to greigite ($y = 0$) and violarite ($y = 1$). (b) The free energy of mixing $\Delta G_{mix}(y)$ calculated with respect to greigite ($y = 0$) and violarite ($y = 1$) at a range of different temperatures.

plains why at this low concentration, substitution of Ni into a tetrahedral site in greigite will lead to a greater reduction in cell parameter than for the equivalent octahedral site substitution.

These geometrical effects link in with the results displayed in Fig. 5, which shows that substitution of the first 8 Ni into the greigite unit cell leads to a sharp decrease in the cell parameter, by a value of approximately 0.366 Å. Yet substitution of a further 8 Ni (to form violarite) is accompanied by

Table 2
Relaxation geometries from DFT calculations.

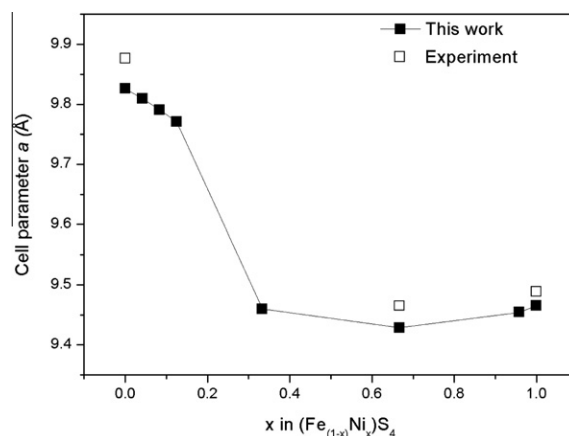| Structure	Cell parameter a (to 3 s.f.)	Bond type	Length (Å)
$Fe_{24}S_{32}$	9.83	Fe_A–S	2.199
		Fe_B–S	2.413
$Ni_{24}S_{32}$	9.47	Ni_A–S	2.190
		Ni_B–S	2.289
$Ni_AFe_{23}S_{32}$	9.77	Ni_A–S	2.175
		Fe_B–S($-Ni_A$)	2.387
$Ni_BFe_{23}S_{32}$	9.80	Ni_B–S	2.399
		Fe_B–S($-Ni_B$)	2.433
		Fe_A–S($-Ni_B$)	2.213

Fig. 5. Variation in cell parameter as calculated via DFT methods and the Nearest Neighbour Energy Model, shown alongside experimental results (Craig, 1971).

a further reduction of only 0.032 Å. The implication is again that, as suggested from our DFT calculations, the biggest distortion of the unit cell occurs from occupation of the tetrahedral sites by Ni (we know from our NN model that at a concentration of 8 Ni per unit cell, the Ni will occupy all of the A sites). It should also be noted that the trend exhibited by cell parameter a shows a deviation from Vegard's law, but is supported by experimental measurements (Craig, 1971). Vaughan and Craig (1978) have explained this phenomenon in the context of the number of electrons in the anti-bonding σ^* orbitals. The numbers (per formula unit) for greigite, violarite and polydymite are 7, 4 and 6, respectively. The greater the number of electrons occupying these orbitals, the greater the repulsive effect on the proximal sulphur ligands, and thus the larger the cell parameter.

4. CONCLUSIONS

We have shown here that partitioning of Ni between tetrahedral and octahedral sites in Fe–Ni thiospinels, $(Fe_{1-x}Ni_x)_3S_4$, is strongly dependent on the composition. At low concentrations ($x < 0.2$) there is a strong preference for octahedral (B) site occupation of Ni. This is an interesting result because it somehow breaks the analogy between Ni-doped greigite and biological enzymes with (Fe, Ni)S clusters, where Ni is usually tetra-coordinated (Volbeda et al., 1995; Dobbek et al., 2001; Volbeda and Fontecilla-Camps, 2003, 2005; Svetlitchnyi et al., 2004; Ragsdale, 2009; Gencic et al., 2010). The analogy in coordination environment is better for the thiospinels with higher Ni concentrations ($x > 0.25$), for which Ni ions locate preferentially in the tetrahedral (A) sites.

It should also be noted that in enzymes such as CODH, there are four Fe ions and only one Ni ion in the active C-cluster (Dobbek et al., 2001; Thauer, 2001; Ragsdale, 2009), which partly explains why the iron–sulphur membrane theory papers refer to Ni-doped greigite rather than violarite, which has a higher Ni/Fe ratio. Yet $(Fe_{1-x}Ni_x)_3S_4$ minerals with a low concentration of nickel are not very abundant or are not well documented, which coincides with

our own results, showing that Ni doping of greigite is highly unstable with respect to separation into a violarite phase.

Our results raise the issue of whether $(Fe, Ni)_3S_4$ thiospinels with higher Ni content, rather than low-Ni greigite, should be considered as responsible for the catalytic activity mimicking the role of enzymes in existing theories of the origin of life.

ACKNOWLEDGMENTS

REFERENCES

Blöchl P. E. (1994) Projector augmented-wave method. *Phys. Rev. B* **50**, 17953–17979.

Canaguier S., Artero V. and Fontecave M. (2008) Modelling NiFe hydrogenases: nickel-based electrocatalysts for hydrogen production. *Dalton Trans.*, 315–325.

Cody G. D. (2004) Transition metal sulfides and the origins of metabolism. *Ann. Rev. Earth Planet. Sci.* **32**, 569–599.

Craig J. R. (1971) Violarite stability relations. *Am. Mineral.* **56**, 1303–1311.

Devey A. J. and de Leeuw N. H. (2010) Density functional theory study of the high- and low-temperature phases of cubic iron sulfide. *Phys. Rev. B* **82**, 235112.

Devey A. J., Grau-Crespo R. and de Leeuw N. H. (2008) Combined density functional theory and interatomic potential study of the bulk and surface structures and properties of the iron sulfide mackinawite (FeS). *J. Phys. Chem. C* **112**, 10960–10967.

Devey A. J., Grau-Crespo R. and de Leeuw N. H. (2009) Electronic and magnetic structure of Fe_3S_4: GGA + U investigation. *Phys. Rev. B* **79**, 195126.

Dobbek H., Svetlitchnyi V., Gremer L., Huber R. and Meyer O. (2001) Crystal structure of a carbon monoxide dehydrogenase reveals a [Ni–4Fe–5S] cluster. *Science* **293**, 1281–1285.

Ferry J. G. (1995) CO dehydrogenase. *Ann. Rev. Microbiol.* **49**, 305–333.

Freke A. M. and Tate D. (1961) Formation of magnetic iron sulphide by bacterial reduction of iron solutions. *J. Biochem. Microbiol. Technol. Eng.* **3**, 29.

Gencic S., Duin E. C. and Grahame D. A. (2010) Tight coupling of partial reactions in the acetyl-coa decarbolase/synthase (ACDS) multienzyme complex from methanosarcina thermophila acetyl C–C bond fragmentation at the a cluster promoted by protein conformational changes. *J. Biol. Chem.* **285**, 15450–15463.

Grau-Crespo R., Al-Baitai A. Y., Saadoune I. and De Leeuw N. H. (2010) Vacancy ordering and electronic structure of gamma-Fe_2O_3 (maghemite): a theoretical investigation. *J. Phys. Condensed Matter* **22**, 255401.

Grau-Crespo R., de Leeuw N. H. and Catlow C. R. A. (2003) Cation distribution and magnetic ordering in $FeSbO_4$. *J. Mater. Chem.* **13**, 2848–2850.

Grau-Crespo R., de Leeuw N. H. and Catlow C. R. A. (2004) Distribution of cations in $FeSbO_4$: a computer modeling study. *Chem. Mater.* **16**, 1954–1960.

Grau-Crespo R., Hamad S., Catlow C. R. A. and de Leeuw N. H. (2007) Symmetry-adapted configurational modelling of fractional site occupancy in solids. *J. Phys. Condensed Matter* **19**, 256201.

Hoffmann V. (1992) Greigite (Fe_3S_4) – magnetic-properties and 1st domain observations. *Phys. Earth Planet. In.* **70**, 288–301.

Huber C. and Wächtershäuser G. (1997) Activated acetic acid by carbon fixation on (Fe, Ni)S under primordial conditions. *Science* **276**, 245–247.

Kresse G. and Furthmüller J. (1996) Efficient iterative schemes for ab initio total-energy calculations using a plane-wave basis set. *Phys. Rev. B* **54**, 11169–11186.

Kresse G. and Hafner J. (1993) Ab initio molecular-dynamics for liquid–metals. *Phys. Rev. B* **47**, 558–561.

Kresse G. and Hafner J. (1994) Ab-initio molecular-dynamics simulation of the liquid–metal amorphous-semiconductor transition in germanium. *Phys. Rev. B* **49**, 14251–14269.

Kresse G. and Joubert D. (1999) From ultrasoft pseudopotentials to the projector augmented-wave method. *Phys. Rev. B* **59**, 1758–1775.

Lavrentiev M. Y., Purton J. A. and Allan N. L. (2003) Ordering in spinels – a Monte Carlo study. *Am. Mineral.* **88**, 1522–1531.

Lindahl P. A. (2004) Acetyl-coenzyme a synthase: the case for a Ni–P(0)-based mechanism of catalysis. *J. Biol. Inorg. Chem.* **9**, 516–524.

Metropolis N., Rosenbluth A. W., Rosenbluth M. N., Teller A. H. and Teller E. (1953) Equation of state calculations by fast computing machines. *J. Chem. Phys.* **21**, 1087–1092.

Misra K. C. and Fleet M. E. (1974) Chemical composition and stability of violarite. *Econ. Geol.* **69**, 391–403.

Monkhorst H. J. and Pack J. D. (1976) Special points for Brillouin-zone integrations. *Phys. Rev. B* **13**, 5188–5192.

Perdew J. P., Chevary J. A., Vosko S. H., Jackson K. A., Pederson M. R., Singh D. J. and Fiolhais C. (1992) Atoms, molecules, solids, and surfaces – applications of the generalized gradient approximation for exchange and correlation. *Phys. Rev. B* **46**, 6671–6687.

Purton J. A., Lavrentiev M. Y. and Allan N. L. (2005) Monte Carlo simulation of GaN/InN mixtures. *J. Mater. Chem.* **15**, 785–790.

Ragsdale S. W. (2009) Nickel-based enzyme systems. *J. Biol. Chem.* **284**, 18571–18575.

Rickard D. and Luther G. W. (2007) Chemistry of iron sulfides. *Chem. Rev.* **107**, 514–562.

Rohrbach A., Hafner J. and Kresse G. (2003) Electronic correlation effects in transition-metal sulfides. *J. Phys. Condensed Matter* **15**, 979–996.

Ruiz-Hernandez S. E., Grau-Crespo R., Ruiz-Salvador A. R. and De Leeuw N. H. (2010) Thermochemistry of strontium incorporation in aragonite from atomistic simulations. *Geochim. Cosmochim. Acta* **74**, 1320–1328.

Russell M. J. and Hall A. J. (1997) The emergence of life from iron monosulphide bubbles at a submarine hydrothermal redox and pH front. *J. Geol. Soc.* **154**, 377–402.

Russell M. J. and Martin W. (2004) The rocky roots of the acetyl-CoA pathway. *Trends Biochem. Sci.* **29**, 358–363.

Skinner B. J., Grimaldi F. S. and Erd R. C. (1964) Greigite thiospinel of iron – new mineral. *Am. Mineral.* **49**, 543–555.

Svetlitchnyi V., Dobbek H., Meyer-Klaucke W., Meins T., Thiele B., Romer P., Huber R. and Meyer O. (2004) A functional Ni–Ni-[4Fe–4S] cluster in the monomeric acetyl-CoA synthase from carboxydothermus hydrogenoformans. *Proc. Natl. Acad. Sci. USA* **101**, 446–451.

Tenailleau C., Etschmann B., Ibberson R. M. and Pring A. (2006) A neutron powder diffraction study of Fe and Ni distributions

in synthetic pentlandite and violarite using Ni-60 isotope. *Am. Mineral.* **91**, 1442–1447.

Thauer R. K. (2001) Nickel to the fore. *Science* **293**, 1264–1265.

Vaughan D. J., Burns R. G. and Burns V. M. (1971) Geochemistry and bonding of thiospinel minerals. *Geochim. Cosmochim. Acta* **35**, 365–381.

Vaughan D. J. and Craig J. R. (1978) *Mineral Chemistry of Sulfides*. Cambridge University Press.

Vaughan D. J. and Craig J. R. (1985) The crystal-chemistry of iron–nickel thiospinels. *Am. Mineral.* **70**, 1036–1043.

Volbeda A., Charon M. H., Piras C., Hatchikian E. C., Frey M. and Fontecillacamps J. C. (1995) Crystal structure of the nickel–iron hydrogenase from Desulfovibrio-gigas. *Nature* **373**, 580–587.

Volbeda A. and Fontecilla-Camps J. C. (2003) The active site and catalytic mechanism of nife hydrogenases. *Dalton Trans.*, 4030–4038.

Volbeda A. and Fontecilla-Camps J. C. (2005) Structure–function relationships of nickel–iron sites in hydrogenase and a comparison with the active sites of other nickel–iron enzymes. *Coord. Chem. Rev.* **249**, 1609–1619.

Vosko S. H., Wilk L. and Nusair M. (1980) Accurate spin-dependent electron liquid correlation energies for local spin-density calculations – a critical analysis. *Can. J. Phys.* **58**, 1200–1211.

Waldner P. (2009) Thermodynamic modelling of violarite. *J. Chem. Thermodynam.* **41**, 171–174.

Associate editor: David J. Vaughan